High-Gain 500-GHz InP HBT Power Amplifiers

Jerome Cheron[1,2], Rob D. Jones[1,3], Richard A. Chamberlin[1], Dylan F. Williams[1], Miguel E. Urteaga[4], Kassiopeia Smith[1], Nicholas R. Jungwirth[1], Bryan T. L. Bosworth[1], Christian J. Long[1], Nathan D. Orloff[1], Peter H. Aaen[3] and Ari D. Feldman[1].

1 National Institute of Standards and Technology, Boulder, CO, USA.
2 Department of Physics, University of Colorado, Boulder, CO, USA.
3 Colorado School of Mines, Golden, CO, USA.
4 Teledyne Scientific Company, Thousand Oaks, CA, USA.

***Abstract*— We report two terahertz monolithic integrated circuit (TMIC) amplifiers operating at 500 GHz. The 6-stage single-ended power amplifiers use Teledyne's 130 nm indium-phosphide double heterojunction bipolar transistors in a common-base configuration. The impedance matching networks of the first amplifier are designed with shunt lines while the second amplifier uses shunt metal-insulator-metal capacitors. We measured and compared the small-signal and large-signal performance of the two amplifiers around 500 GHz. Although the two TMICs exhibit a similar transducer gain (24 dB) and output power (up to -0.7 dBm), we obtained better yield with the amplifiers designed with shunt lines.**

Keywords*— *Submillimeter-wave, terahertz monolithic integrated circuit (TMIC), power amplifier, common-base, indium phosphide (InP), double heterojunction bipolar transistor (HBT), WR2.2, WR1.5.

I. Introduction

Terahertz (THz) solid-state technologies operating from 300 GHz to 1 THz [1-3] have found numerous applications in imaging systems, remote sensing, radar and high-speed communications. The possibility of designing ultra-compact multi-functionality monolithic circuits up to 1 THz also enables practical application in instrumentation engineering. The development of novel measurement tools, such as a high-precision source or synthesizer, requires amplifier blocks able to deliver up to milliwatts of output power. However, high output power is not enough. High gain is also required to amplify the low level of terahertz electrical signals, often generated by multiplier chains [4]. One promising approach consists of amplifying the electrical signals generated by optoelectronic devices [5] at the lower end of the terahertz band [5].

THz monolithic integrated circuit (TMIC) amplifiers using a 130 nm double heterojunction bipolar transistor (HBT) technology developed by Teledyne Scientific[1] have been reported up to 670 GHz [1]. In this paper, we use this technology to design two power amplifiers at 500 GHz. We describe the amplifier technology and two different amplifier designs: The first amplifier uses shunt lines while the second TMIC uses shunt Metal-Insulator-Metal (MIM) capacitors. We then simulate and measure the small- and large-signal characteristics of the two amplifiers and compare their output power and transducer gain with other amplifiers published in the literature. We show that while the performance of the amplifiers is comparable, the shunt lines used in the first amplifier allow for more accurate design.

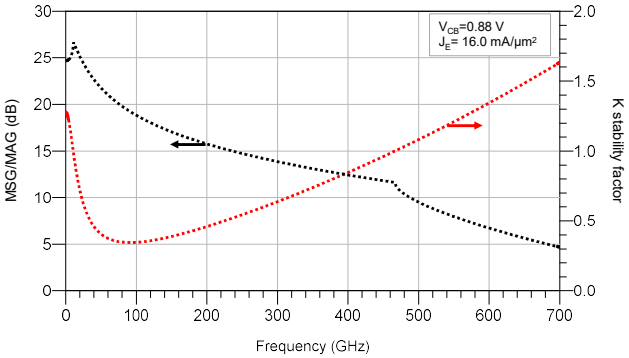

Fig. 1. Simulation of the maximum gain and K-stability factor of a 6 μm long emitter common-base HBT. V_{CB}=0.88 V and J_E= 16 mA/μm².

II. 130 nm InP HBT Technology

The transistors used in this work are epitaxially grown on a 100 mm diameter indium-phosphide (InP) substrate. The HBTs have a common-emitter (CE) breakdown voltage of 3.5 V and a maximum current emitter density J_E = 25 mA/μm² at V_{CE} = 2.0 V As shown in Fig. 1, a 6 μm emitter long transistor in a common-base configuration exhibits a simulated maximum stable gain of 5 dB at 700 GHz.

The technology is described in [1] and a cross section of the passive process is illustrated in Fig. 2(a). The passive circuits are built using 3-levels of interconnects embedded into a 7 μm thick benzo-cyclobutene (BCB) layer. After completing frontside fabrication, the InP substrate is thinned to 75 μm with the option of adding through-substrate vias. For the designs in this work, grounded coplanar waveguide (CPW) lines are formed using the first level of metallization (metal 1) with a continuous ground-plane formed in M3 top metallization. This configuration connects the transistor's terminals to the

[1] We identify commercial products only to accurately describe the experiments and analysis we performed. NIST does not endorse commercial products. Other products may work as well or better.

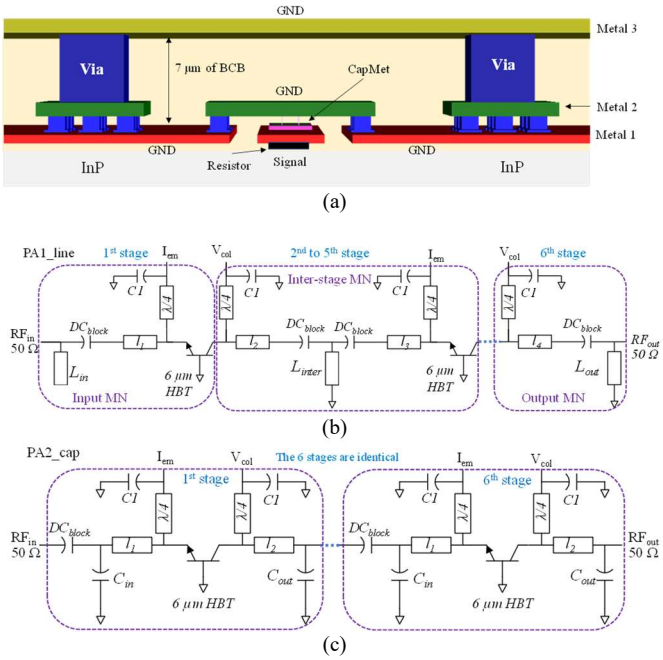

Fig. 2. (a) Cross-section of the TMIC passive process. Circuit schematic of the 6-stage amplifiers designed with (b) shunt lines and with (c) shunt MIM capacitors.

matching network, reducing parasitic elements between the transistor and the circuit. The top metal layer (metal 3) is also connected to the ground plane using interconnect vias through the BCB dielectric. The integrated circuit fabrication process also includes a 0.3 fF/μm^2 MIM capacitor layer and a 50 Ω/sq thin-film resistor layer, which we use in our matching network configurations.

III. TMIC Power-Amplifier Designs

In this study, we aimed to design a common-base power amplifier that delivers 0 dBm of output power with at least 20 dB of transducer gain at 500 GHz. InP HBTs in common-base configuration have been widely used to design amplifiers at submillimeter-wave frequencies [6-9]. However, the stability analysis remains a critical step of the design process. Here, we use a 6 μm emitter long transistor that features ground connections at each side of the base finger. This arrangement reduces the equivalent inductance of the connection between the base of the transistor and the ground plane, and consequently improves the stability of the amplifiers.

The 6 μm emitter long HBT provides a good trade-off between gain and delivered output power. As shown in Fig. 1, a maximum stable gain of 9 dB is simulated at 500 GHz (K>1). The maximum bias point is set to V_{CB}=0.88 V and J_E=16 mA/μm^2 to guarantee that the transistor remains unconditionally stable at 500 GHz. We simulate the *K*-factor [10] and obtain $K > 1$ at frequencies above 475 GHz (see Fig. 1).

We designed two amplifiers. The matching networks of the first amplifier, which we refer to as "PA1_line", uses shunt lines, while the second amplifier, which we refer to as "PA2_cap", uses shunt MIM capacitors.

The circuit schematics of the amplifiers are illustrated in

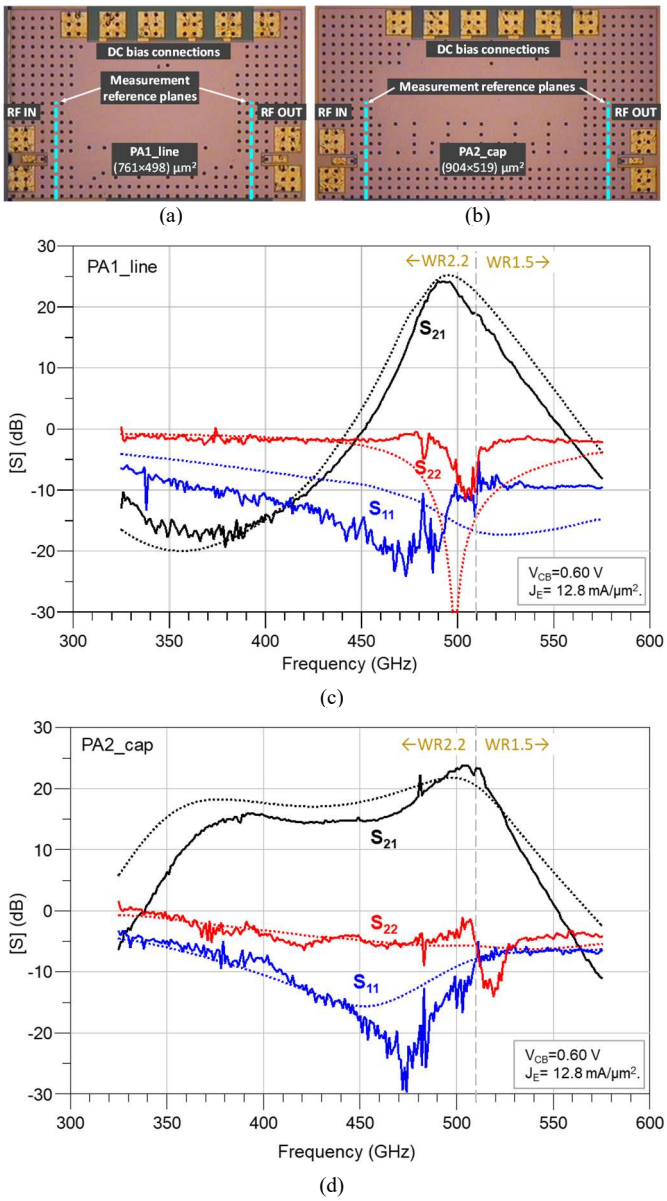

Fig. 3. Photograph of the 6-stage amplifier with (a) shunt lines (PA1_line), and (b) with MIM cap (PA2_cap). Measured (solid line) and simulated (dotted line) S-parameters of the 6-stage amplifiers using (c) shunt lines (PA1_line) and (d) shunt MIM capacitors (PA2_cap). The amplifiers are biased at V_{CB}=0.60 V, J_E= 12.8 mA/μm^2.

Fig. 2(b) and Fig. 2(c). We first designed PA1_line. The output and inter-stage matching networks use shunt lines to ground, while the input matching network is realized with an open stub. The impedances realized by the matching networks of PA1_line are precisely controlled with the shunt lines L_{in}, L_{inter} and L_{out}. Moreover, the electrical response of the grounded CPW lines is not significantly affected by the process variation or the fabrication tolerances.

Although the shunt line topology enables more accurate simulations, it limits the amplifier bandwidth since we use resonant stubs to match the circuits. This topology also requires an extra DC-block in a multi-stage configuration, which increases the total insertion loss of the amplifier.

We adopted a different approach to design of PA2_cap. We

first designed a single-stage amplifier block, matched to 50 Ω at the input and at the output of the circuit. The matching networks of PA2_cap require small values of capacitance. Therefore, we designed a 4.8 fF MIM capacitor at the output (C_{out}) and a 9.6 fF MIM capacitor at the input (C_{in}), corresponding to MIM footprints of 16 μm² and 32 μm², respectively, for the amplifier matching circuits. Then, we cascaded six identical single-stage amplifier blocks in series to form a 6-stage amplifier.

The two amplifiers use identical DC-blocks and bias-Tees. RC networks were also added to the bias-tees of the two amplifiers to improve their low frequency stability (not shown in Fig. 3(b) and Fig. 3(c)).

We used the foundry's non-linear transistor's model to design the amplifiers. The passive elements were simulated using the ADS[1] Momentum software. The last step of the design consisted of a loop gain stability analysis [11] performed at each transistor's terminal of the multi-stage amplifiers. We did not observe any encirclement of the polar point (1,0), which indicates that the simulated amplifiers are stable.

IV. Measurement Results

Photographs of the fabricated 6-stage TMIC power amplifiers are shown in Fig. 3(a) and Fig. 3(b). We used a Keysight PNA-X[1] with the WR2.2 OML[1] and WR1.5 VDI[1] extender heads to measure the S-parameters. We performed the measurements on wafer and applied a multi-line thru-reflect-line (TRL) calibration to define the measurement reference planes directly on the access lines of the circuits, as indicated in Fig. 3(a) and Fig. 3(b).

Large signal measurements were realized with the WR1.5 VDI[1] extender heads at 498 GHz and 520 GHz. We used the Microwave Uncertainty Framework (MUF) [12] software package to perform, 1) a power calibration, using the VDI PM5[1], of the wave-parameters in the waveguide reference planes. For each power level of the PNA-X[1] source that we used during the power sweep characterization, we first performed a power calibration at our two frequencies of interest. Then, 2) we realized an on-wafer TRL calibration and 3), we performed a two-tier calibration with the MUF to de-embed the calibrated waves from the waveguide reference planes to the on-chip reference planes, and to directly measure the input and output power of the amplifiers. We set the IF bandwidth of the PNA-X[1] at 50 Hz. This calibration method allowed us to measure the response of the amplifiers exactly at the frequency of interest, in contrast with the calorimeter power-meter method, which measures the power over the entire bandwidth of the waveguide.

The comparisons between the small-signal measurement results and the simulated performance of the two amplifiers are plotted in Fig. 3(c) and Fig. 3(d). PA1_line and PA2_cap exhibit a small-signal gain higher than 20 dB from 482 GHz to 506 GHz and from 486 GHz to 516 GHz, respectively. We observed good agreement between measurements and simulations even though the measured S_{21} bandwitdh of PA1_line is somewhat narrower than the expected bandwidth. For PA2_cap, we observed somewhat larger differences in the amplitude of S_{21} over the amplifier's passband. We measured the large-signal performance of PA1_line at 498 GHz, for two bias points, and

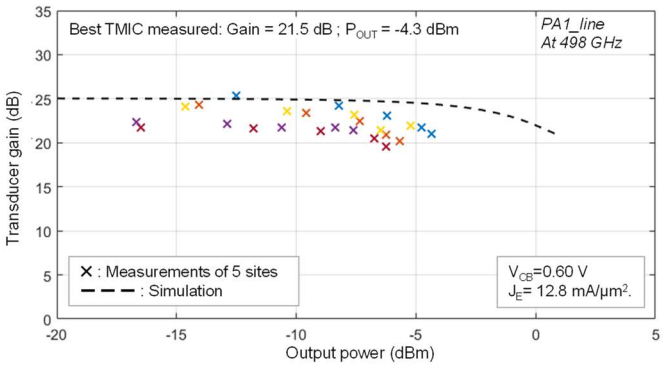

(a)

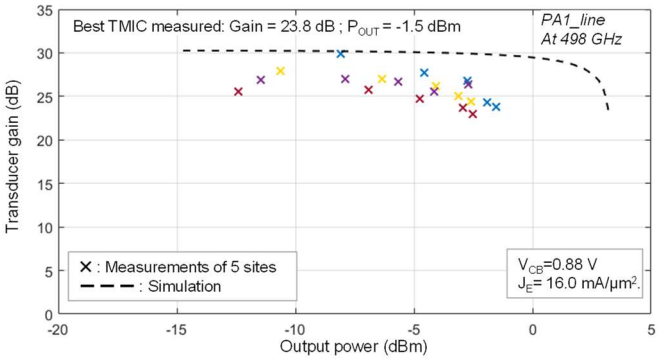

(b)

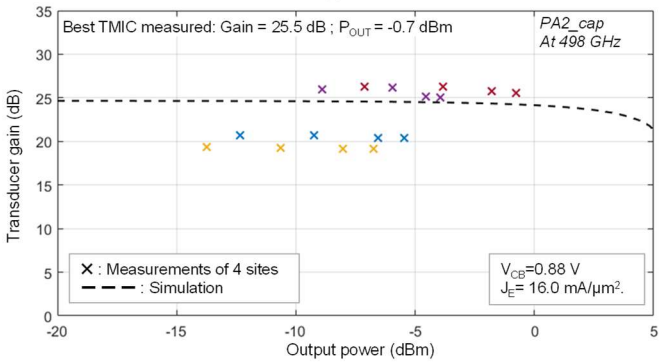

(c)

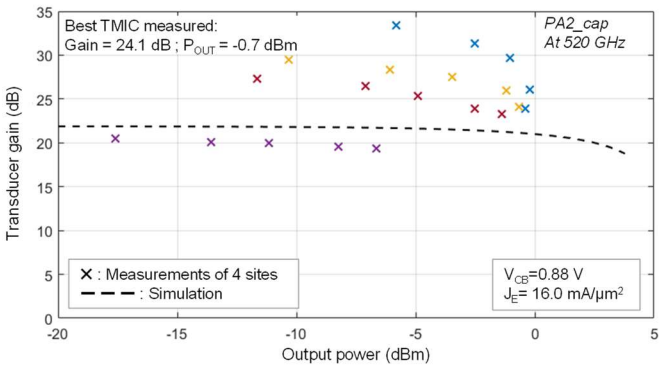

(d)

Fig. 4. Measured (×, one color represents one TMIC) and simulated (dotted line) output power and transducer gain of the 6-stage amplifiers using (a)-(b) shunt lines (PA1_line) at 498 GHz and using MIM capacitors (PA2_cap) at (c) at 498 GHz and (d) at 520 GHz. The amplifiers are biased at V_{CB}=0.60 V, J_E= 12.8 mA/μm² in (a) and at V_{CB}=0.88 V, J_E= 16.0 mA/μm² in (b), (c) and (d).

TABLE I

MEASURED OUTPUT POWER OF AMPLIFIERS FROM 400 GHZ TO 700 GHZ

Ref.	Frequency (GHz)	Output Power (dBm)	Transducer gain (dB)	Technology	Measured performance	year
[13]	395	+1.5	16.5	35 nm InGaAs mHEMT	On-wafer	2020
[14]	417	+7.1	4.8	25 nm InP HEMT	Module	2017
[15]	440	-8	-	35 nm InGaAs mHEMT	On-wafer	2013
[16]	475	-1.1	9.9	60 nm InP HEMT	On-wafer	2020
PA1_line	**498**	**-1.5**	**23.8**	**130 nm InP DHBT**	**On-wafer**	**2021**
PA2_cap	**520**	**-0.7**	**24.1**	**130 nm InP DHBT**	**On-wafer**	**2021**
[8]	585	-0.65	20.2	130 nm InP DHBT	On-wafer	2013
[9]	585	+2.8	21	130 nm InP DHBT	On-wafer	2013
[4]	680	+2.5	-	25 nm InP HEMT	Module	2017

on 5 different sites of the wafer. The results are shown in Fig. 4(a) and Fig. 4(b). PA1_line delivers up to -1.5 dBm of output power with a corresponding transducer gain of 23.8 dB at 498 GHz. The measurements are slightly below the simulated performance, but we obtain a very good yield.

The large signal performance of PA2_cap is plotted in Fig. 4(c) and Fig. 4(d). We measured the TMICs on 4 sites, at 498 GHz and 520 GHz. PA2_cap delivers up to -0.7 dBm of output power at both frequencies, with a transducer gain of 25.5 dB at 498 GHz and 24.1 dB at 520 GHz. However, we did not obtain a good yield with PA2_cap.

At these frequencies, small variations of the capacitance can have significant impact on the electrical response of the amplifiers and dramatically change their stability conditions. Thus, the parasitics associated with the small footprints of C_{in} and C_{out} may have changed the impedances of the small MIM capacitors in the matching networks.

Note that we were not been able to measure the saturated output power of the amplifiers as the power delivered by the extender heads was not sufficiently high to saturate the amplifiers. Based on the measured transducer gain, we can reasonably assume that the two amplifiers would have delivered over 0 dBm of output power under higher input-power drives.

In Table 1, we compare the delivered output power and the transducer gain of our amplifiers with other work published in the literature. We reference only TMIC amplifiers with measured output power, from 400 GHz to 700 GHz. Although some amplifiers deliver an output power above 0 dBm, both of our amplifiers have significantly higher transducer gain.

V. CONCLUSION

We have demonstrated over 23 dB of transducer gain with a delivered output power approaching 0 dBm at 498 GHz and 520 GHz. The design approach with shunt lines is more robust to process variations and presents very good yield at 498 GHz. We observed more process variations in the TMIC amplifiers designed with small MIM capacitors. We believe that variations in the electrical properties of minimum size MIM capacitors likely impacted the measured electrical performance.

ACKNOWLEDGMENT

The authors would like to thank Dr. Alirio Boaventura, from the National Institute of Standards and Technology (NIST), and Dr. Gustavo Avolio, from Anteverta-mw, for their critical reviews.

REFERENCES

[1] M. Urteaga, Z. Griffith, M. Seo, J. Hacker and M. J. W. Rodwell, "InP HBT Technologies for THz Integrated Circuits," in *Proceedings of the IEEE*, vol. 105, no. 6, pp. 1051-1067, June 2017, doi: 10.1109/JPROC.2017.2692178.

[2] W. Deal, X. B. Mei, K. M. K. H. Leong, V. Radisic, S. Sarkozy and R. Lai, "THz Monolithic Integrated Circuits Using InP High Electron Mobility Transistors," in *IEEE Transactions on Terahertz Science and Technology*, vol. 1, no. 1, pp. 25-32, Sept. 2011, doi: 10.1109/TTHZ.2011.2159539.

[3] A. Tessmann *et al*., "Metamorphic HEMT MMICs and Modules Operating Between 300 and 500 GHz," in *IEEE Journal of Solid-State Circuits*, vol. 46, no. 10, pp. 2193-2202, Oct. 2011, doi: 10.1109/JSSC.2011.2163212.

[4] A. Zamora et al., "A high efficiency 670 GHz x36 InP HEMT multiplier chain," 2017 IEEE MTT-S International Microwave Symposium (IMS), 2017, pp. 977-979, doi: 10.1109/MWSYM.2017.8058752.

[5] A. Mingardi, W-D. Zhang, E. R. Brown, A. D. Feldman, T. E. Harvey, and R. P. Mirin, "High power generation of THz from 1550-nm photoconductive emitters," *Opt. Express 26*, 14472-14478 (2018).

[6] J. Cheron and E. Grossman, "High gain 220GHz power amplifier MMICs with minimal footprint," *2016 IEEE MTT-S International Microwave Symposium (IMS)*, San Francisco, CA, USA, 2016, pp. 1-3, doi: 10.1109/MWSYM.2016.7540038.

[7] J. Cheron et al., " Collector Series-Resistor to Stabilize a Broadband 400 GHz Common-Base Amplifier," submitted in *IEEE Transactions on Terahertz Science and Technology*,

[8] J. Hacker, M. Urteaga, M. Seo, A. Skalare and R. Lin, "InP HBT amplifier MMICs operating to 0.67 THz," 2013 IEEE MTT-S International Microwave Symposium Digest (MTT), Seattle, WA, USA, 2013, pp. 1-3, doi: 10.1109/MWSYM.2013.6697518.

[9] M. Seo et al., "A 600 GHz InP HBT amplifier using cross-coupled feedback stabilization and dual-Differential Power Combining," 2013 IEEE MTT-S International Microwave Symposium Digest (MTT), Seattle, WA, USA, 2013, pp. 1-3, doi: 10.1109/MWSYM.2013.6697692.

[10] J. Rollett, "Stability and Power-Gain Invariants of Linear Twoports," in *IRE Transactions on Circuit Theory*, vol. 9, no. 1, pp. 29-32, March 1962, doi: 10.1109/TCT.1962.1086854.

[11] M. Ohtomo, "Stability analysis and numerical simulation of multidevice amplifiers," in IEEE Transactions on Microwave Theory and Techniques, vol. 41, no. 6, pp. 983-991, June-July 1993, doi: 10.1109/22.238513.

[12] D. F. Williams, B. F. Jamroz and A. Lewandowski. NIST Microwave Uncertainty Framework. Nat. Inst. of Standards and Technol. [Online]. Available: http://www.nist.gov/ctl/rf-technology/related-software.cfm.

[13] B. Gashi et al., "Broadband and High-Gain 400-GHz InGaAs mHEMT Medium-Power Amplifier S-MMIC," 2020 IEEE/MTT-S International Microwave Symposium (IMS), Los Angeles, CA, USA, 2020, pp. 484-487, doi: 10.1109/IMS30576.2020.9223968.

[14] A. Zamora et al., "A Submillimeter Wave InP HEMT Multiplier Chain," in IEEE Microwave and Wireless Components Letters, vol. 25, no. 9, pp. 591-593, Sept. 2015, doi: 10.1109/LMWC.2015.2451364.

[15] U. J. Lewark et al., "A 440 GHz balanced active frequency multiplier-by-four SMMIC," 2013 European Microwave Integrated Circuit Conference, Nuremberg, Germany, 2013, pp. 216-219.

[16] H. Hamada, T. Tsutsumi, H. Matsuzaki, H. Sugiyama and H. Nosaka, "475-GHz 20-dB-Gain InP-HEMT Power Amplifier Using Neutralized Common-Source Architecture," 2020 IEEE/MTT-S International Microwave Symposium (IMS), Los Angeles, CA, USA, 2020, pp. 1121-1124, doi: 10.1109/IMS30576.2020.9223.